Chaos, Solitons and Fractals 168 (2023) 113197

Contents lists available at ScienceDirect

Chaos, Solitons and Fractals

journal homepage: www.elsevier.com/locate/chaos

Spatio-temporal patterns resulting from a predator-based disease with immune prey

Nayana Mukherjee [a], Stacey R. Smith? [b], Mainul Haque [c,*]

[a] Department of Computational Biology, Institute of Mathematical Sciences, Chennai, India
[b] Department of Mathematics and Faculty of Medicine, The University of Ottawa, Ottawa, Canada
[c] School of Mathematical Science, The University of Nottingham, Nottingham, UK

ARTICLE INFO

Keywords:
Predator–prey
Infected predator
Diffusive instability
Travelling waves
Spatio-temporal chaos

ABSTRACT

Propagation of a disease through a spatially varying population poses complex questions about disease spread and population survival. We consider a spatio-temporal predator–prey model in which a disease only affects the predator. Diffusion-driven instability conditions are analytically derived for the spatio-temporal model. We perform numerical simulation using experimental data given in previous studies and demonstrate that travelling waves, periodicity and chaotic patterns are possible. We show that the introduction of disease in the predator species makes the standard Rosenzweig–MacArthur model capable of producing Turing patterns, which is not possible without disease. However, in the absence of infection, both species can coexist in spiral non-Turing patterns. It follows that disease persistence may be predictable, while eradication may not be.

1. Introduction

Infectious diseases pose enormous challenges in nature, at almost every trophic level [1,2]. External factors such as climate change or environmental contaminants are likely to exacerbate such outbreaks in marine mammals, for example [3,4], while infectious agents can disrupt the structure, functioning and stability of food webs [5]. Humans are continually at risk of emerging infectious diseases due to changing environmental patterns [6–8]. Propagation of an infectious disease through a population can have profound effects on both species interaction and also the nature of the disease spread [9].

Mathematical models can provide insights into such intertwined phenomena by mixing both ecological and epidemiological factors [10–12], although such models can be complex. Eco-epidemic models have been used, for example, to understand whether attacking a diseased prey increases the chances of epidemic spreading in a predator or not [13–15]. As per predator–prey interactions, many modelling approaches are prevalent, including various forms of functional responses such as Holling types I, II and III, Ivlev type, Beddington–DeAngelis type, ratio-dependent, et cetera [16]. Compartment models (SIR, SIER, MSEIR, et cetera) are commonly formulated to study epidemic diseases [17], which can be included in predator–prey modelling, with disease in either or both species [18,19].

Examples of infectious diseases affecting land-based predator hosts include rabies infecting foxes; *Sarcoptes* spp. affecting both foxes and coyotes; Yersinia pestis infecting prairie dogs; Stomoxys calcitrans affecting lions; and *Aeromonas hydrophila* infecting alligators. In the marine environment, we mention Phocine distemper virus affecting both the common seal and the striped dolphin [20].

Spatio-temporal pattern formation has been studied for ecological and epidemiological problems as well as combinations of the two. The spread of a disease within either a single-species population or in multi-species populations may require the disease to be considered on a spatial domain [21]. Due to the spatial heterogeneity, populations tend to localize on the spatial domain, resulting in pattern emergence. Some patterns can be ecologically interpreted as isolated patches of high population density surrounded by low population densities in the neighbouring areas or vice versa. Others are interlaced bands of high or low population densities. Some are non-stationary with respect to space and time, where the species populations move from one region to another either periodically or aperiodically [22–26].

Reaction–diffusion equations are used to mathematically model such eco-epidemiological scenarios [27]. These are continuous-space/continuous-time models and can be single species, two species or multispecies models; depending on instability conditions, various types of patterns are generated [28]. Three-species population models include two prey and one predator, one prey and two predators or predator–prey/top-predator type, cyclic competitor etc. The disease may affect one or more of these species; in the case of limited infections, a natural

* Corresponding author.
E-mail address: Mainul.Haque@nottingham.edu.cn (M. Haque).

https://doi.org/10.1016/j.chaos.2023.113197
Received 7 December 2022; Received in revised form 7 January 2023; Accepted 24 January 2023
Available online 6 February 2023
0960-0779/© 2023 Elsevier Ltd. All rights reserved.

question is whether a particular disease will become an epidemic through predator–prey interactions and how this might change the structure of the species interactions. Modelling can help determine whether the introduction of a new disease can lead to an epidemic due to species interaction or, conversely, whether an existing epidemic will come to an end [29].

Here, we consider an eco-epidemic model in which the predator population is infected with a disease; the predator population consumes its resources from non-diseased prey, although it has an additional option for food as well. We examine this model in two spatial dimensions and study the pattern-formation possibilities for the entire nonlinear spatio-temporal model. This paper is organized as follows. In Section 2, we develop the spatio-temporal model and describe the respective parameters and variables. In Section 3, we derive analytical results, including diffusion-driven instability. In Section 4, we illustrate our theoretical results with numerical simulations. We conclude with a discussion.

2. The spatio-temporal eco-epidemic model

We consider a predator–prey model where the predator is infected with a disease [30,31]. We assume that predators can spread the disease amongst themselves but not amongst the prey. The prey population is described using logistic growth and is subject to infections caused by susceptible predators at rate M and by infected predators at rate P. Moreover, the species-interaction terms show a saturation effect for both types of predators. which may have alternate food sources, represented by parameter B [32–34].

Consider a two-dimensional bounded spatial domain Ω with boundary $\partial\Omega$. Denote the prey population density by $X(x_1, x_2, \tau)$, the susceptible predator population by $Y(x_1, x_2, \tau)$ and the infected predator population by $Z(x_1, x_2, \tau)$. The time variable is τ, and the space variables are (x_1, x_2). Natural mortality q and disease-induced mortality δ are also incorporated. We consider random diffusion of prey and predator populations in the spatial domain. The spatio-temporal model is then

$$\frac{\partial X}{\partial \tau} = D_1 \Delta X + X\left(R - bX - \frac{MY}{A+X} - \frac{PMZ}{A+X}\right), \tag{1a}$$

$$\frac{\partial Y}{\partial \tau} = D_2 \Delta Y + Y\left(\frac{E_1 MX}{A+X} - A_1 Z - q + B\right), \tag{1b}$$

$$\frac{\partial Z}{\partial \tau} = D_3 \Delta Z + Z\left(A_1 Y + \frac{E_1 MPX}{A+X} - q - \delta\right). \tag{1c}$$

Here R is the intrinsic growth rate of the prey, b is the inverse of the carrying capacity of prey population, and the half saturation constant for predator population is given by A. Parameter A_1 is the between-predator transmissibility, and E_1 is the conversion efficiency, which describes prey biomass being converted to predator biomass. The diffusion coefficients for the prey, susceptible predator and infected predator populations are D_1, D_2 and D_3, respectively, while the Laplacian is given by $\Delta \equiv \frac{\partial^2}{\partial x_1^2} + \frac{\partial^2}{\partial x_2^2}$.

We nondimensionalize this model using transformations $\bar{d} \equiv q + \delta$ and $\mu \equiv -q+B$, which can be of either sign. The new variables are of the form $X = Ax, Y = Ay, Z = Az$ and $\tau = \frac{t}{E_1 M}$. The nondimensionalized model is then

$$\frac{\partial x}{\partial t} = d_1 \Delta x + x\left(r - Hx - \frac{ay}{1+x} - \frac{pz}{1+x}\right), \tag{2a}$$

$$\frac{\partial y}{\partial t} = d_2 \Delta y + y\left(\frac{ax}{1+x} - mz + n\right), \tag{2b}$$

$$\frac{\partial z}{\partial t} = d_3 \Delta x + ez\left(my + \frac{px}{1+x} - d\right), \tag{2c}$$

where $r = \frac{R}{E_1 M}$, $H = \frac{Ab}{E_1 M}$, $p = \frac{P}{eE_1 M}$ $m = \frac{A_1 A}{eM}$, $d = \frac{\bar{d}}{eE_1 M}$ and $n = \frac{\mu}{E_1 M}$. We impose initial conditions and zero-flux boundary conditions as follows:

$$x(x_1, x_2, 0) \geq 0, y(x_1, x_2, 0) \geq 0, z(x_1, x_2, 0) \geq 0 \quad (x_1, x_2) \in \Omega, \tag{3a}$$

$$\frac{\partial x}{\partial \nu} = \frac{\partial y}{\partial \nu} = \frac{\partial z}{\partial \nu} = 0, \quad (x_1, x_2) \in \partial\Omega,\ t \geq 0, \tag{3b}$$

where $\bar{x}_1 = \frac{x_1}{\sqrt{x_1^2+x_2^2}}$, $\bar{x}_2 = \frac{x_2}{\sqrt{x_1^2+x_2^2}}$, $d_1 = \frac{D_1}{\sqrt{x_1^2+x_2^2}}$, $d_2 = \frac{D_2}{\sqrt{x_1^2+x_2^2}}$ and $d_3 = \frac{D_3}{\sqrt{x_1^2+x_2^2}}$. We remove the overbars without loss of generality. Here Ω is a closed rectangular region with boundary $\partial\Omega$ and the derivative along the unit outward normal vector to $\partial\Omega$ is $\frac{\partial}{\partial \nu}$.

3. Analytical results

3.1. Non-negativity of solutions

We first establish conditions for non-negativity of solutions.

Lemma 3.1. *Assume that $x(x_1, x_2, t)$ satisfies*

$$\frac{\partial x}{\partial t} - \Delta x = x(r - Hx), \quad (x_1, x_2) \in \Omega,\ t > 0,$$

subject to the boundary condition $\frac{\partial x}{\partial \nu} = 0$ for $(x_1, x_2) \in \partial\Omega$ and initial condition $x(x_1, x_2, 0) > 0$, $(x_1, x_2) \in \Omega$. Then

$$\lim_{t\to\infty} x(x_1, x_2, t) = 1.$$

Theorem 3.2. *All solutions of system (2) with nonnegative initial conditions are nonnegative for $t \geq 0$. Furthermore, the nonnegative solutions (x, y, z) satisfy*

$$\limsup_{t\to\infty} x \leq \frac{r}{H}, \quad \limsup_{t\to\infty} y \leq K_1, \quad \limsup_{t\to\infty} z \leq K_2.$$

Proof. Using the nonnegativity of x and y we have

$$x\left(r - Hx - \frac{ay}{1+x} - \frac{pz}{1+x}\right) \leq x(r - Hx).$$

From Lemma 3.1, there exists a $T_1 > 0$ such that

$$x \leq \frac{r}{H} + \epsilon$$

in $\Omega \times [T_1, \infty)$ for an arbitrary $\epsilon > 0$. For the estimates of y and z, let $\int_\Omega x(X,t) = U_1(t)$, $\int_\Omega y(X,t) = U_2(t)$ and $\int_\Omega z(X,t) = U_3(t)$ where $X \equiv (x_1, x_2)$. Then

$$\frac{dU_1}{dt} = \int_\Omega \frac{\partial x}{\partial t} dX = \int_\Omega d_1 \Delta x dX + \int_\Omega x(r - Hx) dX - \int_\Omega \frac{axy}{1+x} dX - \int_\Omega \frac{pxz}{1+x} dX, \tag{4a}$$

$$\frac{dU_2}{dt} = \int_\Omega \frac{\partial y}{\partial t} dX = \int_\Omega d_2 \Delta y dX + nU_2 + \int_\Omega \frac{axy}{1+x} dX - \int_\Omega mxz dX, \tag{4b}$$

$$\frac{dU_3}{dt} = \int_\Omega \frac{\partial z}{\partial t} dX = \int_\Omega d_3 \Delta z dX - deU_3 + \int_\Omega \frac{epxz}{1+x} dX. \tag{4c}$$

Adding ((4)a) to ((4)b) and using the Neumann boundary conditions, we obtain

$$\begin{aligned}\frac{d}{dt}(U_1 + U_2) &= nU_2 + \int_\Omega x(r - Hx) dX - \int_\Omega \frac{pxz}{1+x} dX - \int_\Omega mxz dX \\ &\leq nU_2 + \int_\Omega x(r - Hx) dX \\ &\leq n(U_1 + U_2) + \left(\frac{r}{H} - n\right) U_1.\end{aligned}$$

Since $\limsup_{t\to\infty} u_1(X,t) \leq \frac{r}{H}$, we have $\limsup_{t\to\infty} U_1(t) \leq \frac{r}{H}|\Omega|$. Thus, for small $\epsilon > 0$, there exists $T_2 > 0$ such that

$$\frac{d}{dt}(U_1 + U_2) \leq n(U_1 + U_2) + \left(\frac{r}{H} - n\right)(1 + \epsilon)|\Omega|$$

for $t > T_2$. Integration leads to

$$\int_\Omega y(X,t) dX = U_2(t) < U_1(t) + U_2(t) \leq \left(\frac{r}{H} - n\right)(1 + \epsilon)|\Omega|, \quad t > T_3$$

for $T_3 > T_2$. This implies that

$$\limsup_{t\to\infty} \int_\Omega y(X,t) dX \leq \left(\frac{r}{H} - n\right)(1 + \epsilon)|\Omega|.$$

Thus, any solution $y(X,t)$ satisfies an L^1 *a priori* estimate $K_{1a} = \left(\frac{r}{H} - n\right)(1+\epsilon)|\Omega|$ for large t which depends on r, H, n and Ω. Furthermore, we can use this L^1 bound to obtain an L^∞ bound K_{1b} for large $t > 0$. (See Theorem 3.1 of Alikakos [35].) Using Lemma 4.7 of Cantrall et al. [36], we can prove that when $d_2 > d_{2*}$, an L^∞ bound K_{1c} occurs depending on K_{1a}. Therefore, there exists $K_1 > 0$ depending only on a lower bound of d_2, such that

$$\limsup_{t\to\infty} y \le K_1.$$

Multiplying ((4)a) by e, ((4)b) by e and adding them to ((4)c), and using the Neumann boundary conditions, we get

$$\begin{aligned}\frac{d}{dt}(U_3 + eU_2 + eU_1) &= e\int_\Omega u_1(r - Hx)dX + neU_2 - deU_3 - \int_\Omega mxz dX\\ &\le eU_1 + neU_2 - deU_3\\ &= (U_3 + eU_2 + eU_1) - (1+de)U_3 + (n-1)eU_2\\ &\le (U_3 + eU_2 + eU_1) + neU_2.\end{aligned}$$

We know that $\limsup_{t\to\infty} U_1(t) \le \frac{r}{H}|\Omega|$ and $\limsup_{t\to\infty} U_2(t) \le \left(\frac{r}{H} - n\right)(1+\epsilon)|\Omega|$. Thus, for small $\epsilon > 0$, there exists $T_4 > 0$ such that

$$\frac{d}{dt}(U_3 + eU_2 + eU_1) \le (U_3 + eU_2 + eU_1) + ne\left(\frac{r}{H} - n\right)(1+\epsilon)|\Omega|$$

holds for $t > T_4$. Integration leads to

$$\begin{aligned}\int_\Omega u_3(X,t)dX = U_3(t) &< U_3(t) + eU_2(t) + eU_1(t),\\ &\le ne\left(\frac{r}{H} - n\right)(1+\epsilon)|\Omega|\end{aligned}$$

for $T_5 > T_4$. Thus, any solution $z(X,t)$ satisfies an L^1 *a priori* estimate

$$K_{2a} = ne\left(\frac{r}{H} - n\right)(1+\epsilon)|\Omega|$$

for large t, which depends on b_1, b_2, a_2, a_4 and Ω. Furthermore, we can use this L^1 bound to obtain an L^∞ bound K_{2b} for large $t > 0$. (See Theorem 3.1 of Alikakos [35].) Using Lemma 4.7 of Cantrell et al. [36] again, we can prove that when $d_3 > d_{3*}$, an L^∞ bound K_{2c} occurs depending on K_{2a}. Therefore, there exists $K_2 > 0$ depending only on a lower bound of d_3, such that

$$\limsup_{t\to\infty} z \le K_2. \quad \square$$

3.2. Diffusion-drive instability conditions

Diffusion-driven instability occurs when the stable homogeneous steady-state becomes unstable due to small perturbations. We take $x(x_1,x_2,t) \equiv x_*$, $y(x_1,x_2,t) \equiv y_*$, $z(x_1,x_2,t) \equiv z_*$ to be the homogeneous steady state for (2). By applying small perturbations to the homogeneous steady state, we have

$$\begin{aligned}\begin{pmatrix} x\\ y\\ z\end{pmatrix} &= \begin{pmatrix} x_*\\ y_*\\ z_*\end{pmatrix} + \epsilon\begin{pmatrix}\hat{u}_1\\ \hat{u}_2\\ \hat{u}_3\end{pmatrix}\exp(\lambda t + i\mathbf{k}\cdot\mathbf{r}) + c.c.\\ &\equiv \begin{pmatrix} x_*\\ y_*\\ z_*\end{pmatrix} + \begin{pmatrix} u(x_1,x_2,t)\\ v(x_1,x_2,t)\\ w(x_1,x_2,t)\end{pmatrix},\end{aligned}$$

where $0 < \epsilon \ll 1$, λ is the perturbation growth rate, $\mathbf{r} \equiv (x,y)$ is the position vector and $c.c.$ represents the complex conjugate. The wave number vector is $\mathbf{k}$, with the wave number given by $k = |\mathbf{k}|$. The characteristic equation for the growth rate λ is determined from $\det(\mathbf{J}_1) = 0$, where

$$\mathbf{J}_1 = \begin{pmatrix} F_1 - d_1k^2 - \lambda & F_2 & F_3\\ G_1 & 0 - d_2k^2 - \lambda & G_3\\ H_1 & H_2 & 0 - d_3k^2 - \lambda\end{pmatrix},$$

with

$$F_1 = -Hx_* + \frac{ax_*y_*}{(1+x_*)^2} + \frac{px_*z_*}{(1+x_*)^2}, \qquad G_1 = \frac{ay_*}{(1+x_*)} - \frac{ax_*y_*}{(1+x_*)^2},$$

$$F_2 = -\frac{ax_*}{(1+x_*)}, \qquad G_3 = -my_*,$$

$$F_3 = -\frac{px_*}{(1+x_*)},$$

$$H_1 = ez_*\left(\frac{p}{(1+x_*)} - \frac{px_*}{(1+x_*)^2}\right),$$

$$H_2 = ez_*m.$$

The characteristic equation is

$$\lambda^3 + A(k^2)\lambda^2 + B(k^2)\lambda + C(k^2) = 0, \tag{5}$$

where

$$\begin{aligned}A(k^2) &= d_2d_3k^4 + k^2(d_1 + d_2 + d_3) - F_1,\\ B(k^2) &= k^4(d_1d_3 + d_1d_2) - k^2(d_3 + d_2)F_1 - G_3H_3 - F_2G_1 - F_3H_1,\\ C(k^2) &= d_1d_2d_3k^6 - d_2d_3F_1k^4 - k^2(d_1G_3H_3 + d_2F_3H_1 + d_3F_2G_1)\\ &\quad - F_2G_3H_1 - F_3G_1H_3 + F_1G_3H_3.\end{aligned}$$

In order to have $\Re(\lambda) < 0$, we require the Routh–Hurwitz criterion to be satisfied, given by:

$$A(k^2) > 0, \quad C(k^2) > 0, \quad A(k^2)B(k^2) - C(k^2) > 0.$$

If this occurs, the homogeneous steady state will be stable. Diffusion-driven instability will manifest when $\Re(\lambda_{\max}) > 0$. Therefore, if λ_1, λ_2, λ_3 are the roots of (5), then we have

$$\begin{aligned}\lambda_1 + \lambda_2 + \lambda_3 &= -A(k^2),\\ \lambda_1\lambda_2 + \lambda_2\lambda_3 + \lambda_3\lambda_1 &= B(k^2),\\ \lambda_1\lambda_2\lambda_3 &= -C(k^2),\\ -(\lambda_1 + \lambda_2)(\lambda_2 + \lambda_3)(\lambda_3 + \lambda_1) &= A(k^2)B(k^2) - C(k^2).\end{aligned}$$

At the bifurcation threshold $k = k_T$, one of the eigenvalues is zero, say λ_1. Hence

$$\lambda_1\Big|_{k^2=k_T^2} = 0, \quad \Re\left(\lambda_2\Big|_{k^2=k_T^2}\right) < 0 \quad \text{and} \quad \Re\left(\lambda_3\Big|_{k^2=k_T^2}\right) < 0. \tag{7}$$

It follows that $C(k_T^2) = 0$. Due to the conditions of diffusion-driven instability given in (7), we get $A(k_T^2) > 0$, $B(k_T^2) > 0$ and $A(k_T^2)B(k_T^2) - C(k_T^2) > 0$. It follows that we have stability if $C(k^2) > 0\ \forall\ k$ and instability if $\exists\ k$ such that $C(k^2) < 0$. The expression can be rewritten as

$$C(k^2) = C_1(k^2)^3 + C_2(k^2)^2 + C_3(k^2) + h,$$

where $C_1 > 0$, since the self-diffusion coefficients are positive and $h > 0$ from the second condition of (3.8). When $k = k_T$, C reaches a minimum, where

$$k_T^2 = \frac{-C_2 + (C_2^2 - 3C_1C_3)^{\frac{1}{2}}}{3C_1}$$

and $\frac{dC(k_T^2)}{d(k_T^2)} = 0$ and $\frac{d^2C(k_T^2)}{d(k_T^2)^2} > 0$. Finally, k_T^2 is positive if $C_3 < 0$ or $C_2 < 0$ and $C_2^2 > 3C_1C_3$. The bifurcation boundary is thus described by

$$2C_2^3 - 9C_1C_2C_3 - 2(C_2^2 - 3C_1C_3)^{\frac{3}{2}} + 27C_1^2h = 0.$$

This derives the conditions for diffusion-driven instability.

4. Numerical simulations

4.1. Eco-epidemiological model

In this section, we perform numerical simulations of system (1) using experimental data from Tanner [31]. Tanner calculated the intrinsic growth rates of some predator and prey populations[1] and divided them

[1] For details, see Page 861.

Table 1
Growth rates per year of some predator–prey interactions [31].

	Species	Observed growth rate	Maximum growth rate
(a)	Muskrat	$0.806 \le r \le 1.068$	$1.101 \le r \le 1.366$
	Mink	$0.022 \le \delta \le 0.185$	$0.378 \le \delta \le 0.531$
(b)	Moose	$0.100 \le r \le 0.127$	$0.171 \le r \le 0.202$
	Wolf	$0.232 \le \delta \le 0.321$	$0.431 \le \delta \le 0.524$
(c)	Snowshoe hare	$0.545 \le r \le 0.810$	$0.769 \le r \le 0.1033$
	Lynx	$\delta \le 0.855$	$\delta \le 1.012$

into three categories: (a) the prey has a higher growth rate than the predator; (b) the predator has a higher growth rate than the prey and (c) both the prey and the predator have approximately equal growth rates as shown in Table 1. Here "observed" means the highest rates reported in the literature and "maximum" means the rates that Tanner judged likely in an optimal environment. In each case, the lower bound is under "observed" fertility and the upper bound is under "maximum" fertility. We have taken the birth rate of the species from the table and keep their variations with this experimental range.

We performed numerical simulations of the model on a square lattice mesh with $\Delta x_1 = \Delta x_2 = 1$ and $\Delta t = 0.01$ using the forward Euler method for the temporal part and a five-point stencil finite-difference scheme for the diffusion part. The results were verified using other choices of Δx_1, Δx_2 and Δt, and no meaningful changes were observed.

Ideally, with the initial conditions as random perturbation to the homogeneous steady state, we should get stationary or non-stationary patterns. However, with the parameter sets we use here, only periodic solutions with respect to space and time are observed, with the homogeneous solution oscillating between two values. By changing the initial conditions, we observe some inhomogeneous spatial patterns. The initial conditions are

$$\begin{aligned} x(x_1, x_2, 0) &= x_* - (2\times 10^{-9})(x_1 - 50)(x_2 - 30) \\ &\quad - (3\times 10^{-5})(x_1 - 50)(x_2 - 30), \\ y(x_1, x_2, 0) &= y_* - (1.2\times 10^{-4})(x_1 - 100) - (6\times 10^{-4})(x_2 - 100), \\ z(x_1, x_2, 0) &= z_* - (1.2\times 10^{-4})(x_1 - 100) - (6\times 10^{-4})(x_2 - 100). \end{aligned}$$

The parameter set is $e = 0.00001, r = 0.89, H = 0.05, m = 0.99, n = 0.05, p = 2.15, d = 3.5, d_1 = 1, d_3 = 0.5$, Diffusion-driven instability conditions are satisfied by this parameter set. We vary a and d_3 to get the bifurcation curve as shown in Fig. 1. Below the curve, the steady state prevails and no patterns exist, whereas patterns start emerging for parameter values above the curve.

As seen in Fig. 2, with particular initial conditions, travelling-wave solutions appear, which form a continuous peak of high population density, travel through the domain and break into two. They again join as time evolves, giving the travelling wavefront solution. It follows that, depending on the diffusivities and initial conditions, the disease can oscillate periodically over time. The patterns in x and y are more prominent than those for z because of the parameter e associated with Eq. (2)(c). Due to the low value of e, the patterns are barely visible for z. Otherwise, if e is not included in the model, the diffusivity d_3 needs to be much higher than that of d_1 and d_2, which is not feasible for numerical simulations, nor is it biologically sensible.

As the value of d_3 increases (keeping other parameter values the same), spiral solutions appear and move out of the system. They can also eventually reappear. The spirals form and break continuously, giving an irregular nature to the solutions. Fig. 3(d) shows the periodic solutions converting to chaotic solutions as d_3 increases. In eco-epidemiological terms, the disease spread becomes unpredictable, unlike the previous case. This model is capable of producing only non-stationary patterns as a result of diffusive instability.

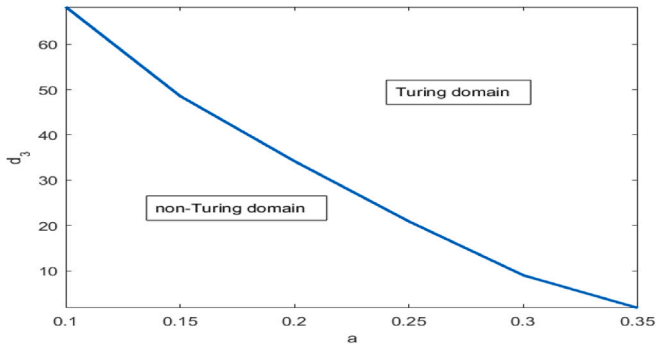

Fig. 1. Bifurcation diagram in the a-d_3 plane showing the diffusion-driven instability curve.

4.2. Disease-free model

Finally, we consider the special case of the model in the absence of disease. In this case, the eco-epidemiological model reduces to an epidemiological one alone. For the disease-free population, we have

$$\frac{\partial x}{\partial t} = d_1 \Delta x + x\left(r - Hx - \frac{ay}{1+x}\right), \tag{9a}$$

$$\frac{\partial y}{\partial t} = d_2 \Delta y + y\left(\frac{ax}{1+x} + n\right). \tag{9b}$$

Model (9) is unable to produce any Turing patterns, with the populations driven to extinction in most cases. However, it produces Turing patterns under cross-diffusions [37].

The perturbations in the corresponding temporal model are described by

$$\begin{pmatrix} x \\ y \end{pmatrix} = \begin{pmatrix} x_* \\ y_* \end{pmatrix} + \begin{pmatrix} C_1 \\ C_2 \end{pmatrix} e^{\lambda t}, \tag{10}$$

where $0 < C_1, C_2 \ll 1$ and λ is the growth rate of perturbations. Substituting (10) into (9), the characteristic equation for the growth rate λ is found from $\det(\mathbf{J}_1) = 0$, where

$$\mathbf{J}_1 = \begin{pmatrix} a_{11} - \lambda & a_{12} \\ a_{21} & -\lambda \end{pmatrix}. \tag{11}$$

Here

$$a_{11} = -Hx_* + \frac{ax_*y_*}{(1+x_*)^2}, \qquad a_{12} = -\frac{ax_*}{(1+x_*)},$$

$$a_{21} = \frac{ay_*}{(1+x_*)} - \frac{ax_*y_*}{(1+x_*)^2}, \qquad a_{22} = 0.$$

The necessary condition for Turing instability is when all the entries of the Jacobian have non-zero entries, with signs given by

$$\begin{pmatrix} + & + \\ - & - \end{pmatrix}, \begin{pmatrix} - & - \\ + & + \end{pmatrix}, \begin{pmatrix} + & - \\ + & - \end{pmatrix} \text{ and } \begin{pmatrix} - & + \\ - & + \end{pmatrix}.$$

Since $a_{22} = 0$, the general Turing instability condition for two species model is not satisfiable. Thus it is impossible to get any Turing patterns for model (1). However, numerical simulations demonstrate that the model is capable of showing non-Turing patterns for lower ranges of diffusivity as shown in Fig. 4. Interacting spiral chaos is observed for the chosen parameter set for low diffusion coefficients. As the range of diffusivities increase, populations are driven to extinction. Introducing the infected predator population into the system, the spirals are lost, but periodic and aperiodic waves are observed, as in the previous cases.

5. Discussion

Eco-epidemic models merge features of two phenomena: the demographics of interacting species and the evolution of epidemics in a composite environment. We considered a spatiotemporal extension to a

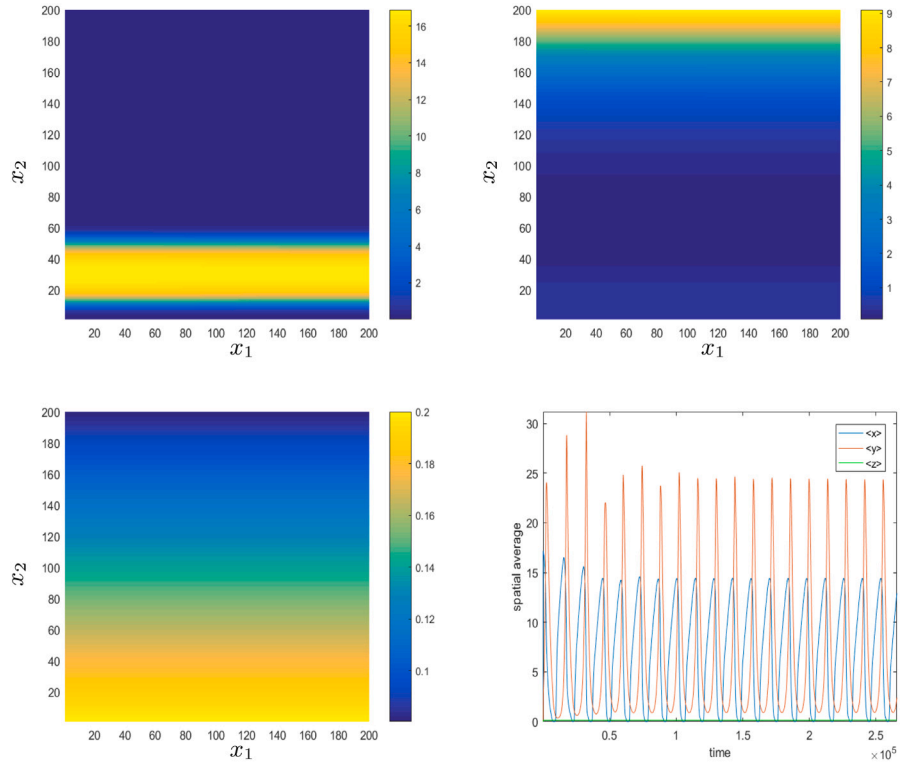

Fig. 2. (a) Plot of x after $t = 700{,}000$ time units. (b) Plot of y after $t = 700{,}000$ time units. (a) Plot of z after $t = 700{,}000$ time units. (d) Plot of spatial averages of x, y and z. The data are $e = 0.00001, r = 0.89, H = 0.05, m = 0.99, n = 0.05, p = 2.15, d = 3.5, a = 0.32, e_1 = 1, e_2 = 1$ and $e_3 = 20$.

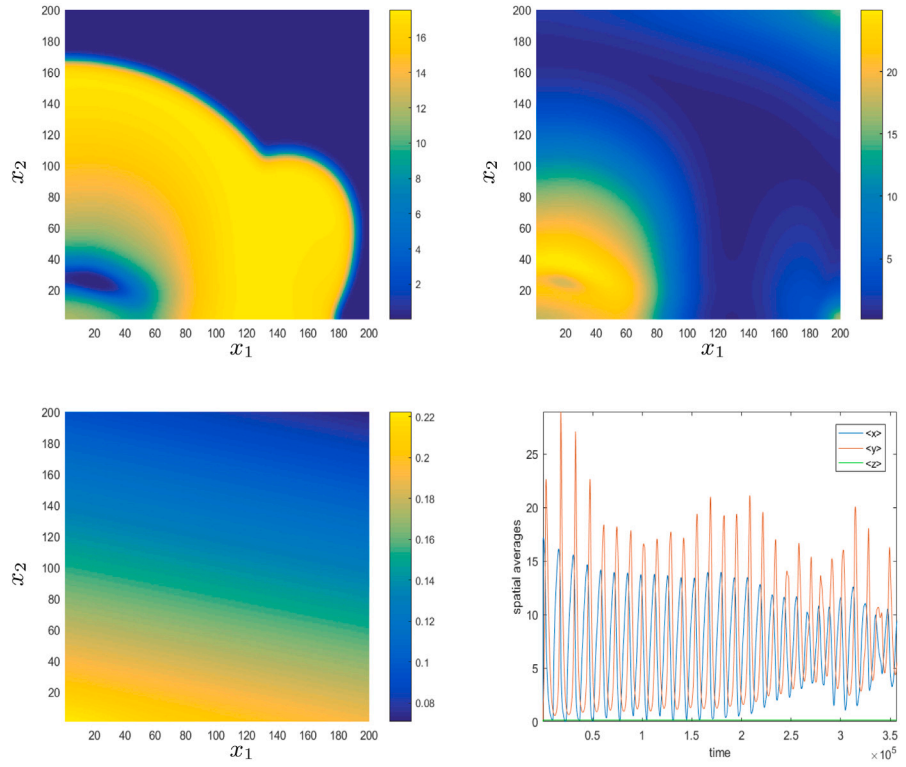

Fig. 3. (a) Plot of x after $t = 700{,}000$ time units. (b) Plot of y after $t = 700{,}000$ time units. (a) Plot of z after $t = 700{,}000$ time units. (d) Plot of spatial averages of x, y and z. The parameter set is as in Fig. 2 except with $e_3 = 80$.

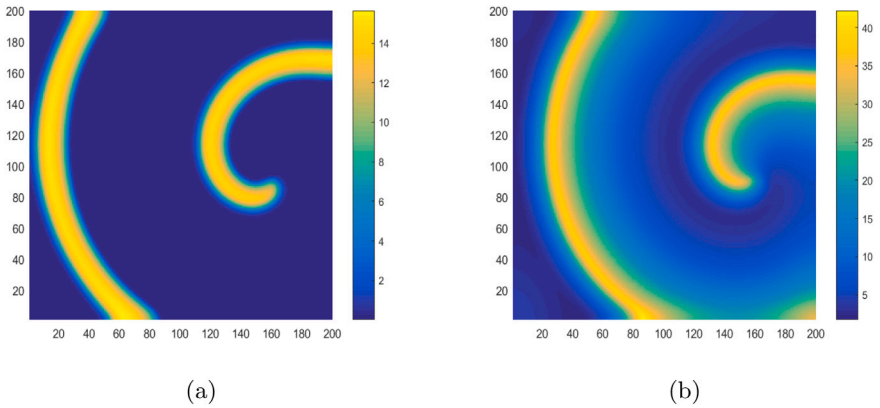

Fig. 4. Spirals in the disease-free model. The parameter set is as in Fig. 2 except with $e_3 = 80$. (a) Plot of x after $t = 700{,}000$ time units; (b) Plot of y after $t = 700{,}000$ time units.

predator–prey population in which some of the predators are infected and the remainder are susceptible using reaction–diffusion equations. We found diffusion-driven instability conditions for the model and generated numerically simulated patterns such as periodic travelling waves and interacting spiral chaos patterns. We also compared the results to the disease-free model and showed that Turing patterns did not occur in this case. It follows that the introduction of a disease in a predator species may bring more complex dynamics to the standard Rosenzweig–MacArthur model.

Due the introduction of the control parameter e, we see z showing almost no Turing patterns. If e is not considered, then the diffusivity of z is too high to see any detailed patterns. The travelling-wave solutions show that the waves of the disease will arrive, peak and then ultimately move out of the spatial domain with time. In this case, the infected predator population will ultimately convert to susceptible and will not lead to an epidemic. The disease will also not spread through the prey population. The disease-free model shows interacting spiral patterns with dynamic predator–prey interactions in which both species co-exist. However, introducing an infected predator changes the course of the dynamics, resulting in travelling wave solutions and chaos.

Note that the high prey population areas correspond to low predator population zones, both for susceptible and infected predator populations. This means that the predator population will attempt to catch the prey from the boundary of prey-rich zones.

Spiral patterns and spiral waves are commonplace in nature, occurring both in biological systems and chemical reactions. The emergence of such spiral patterns suggests that spatial order can emerge from temporal disorder. Fig. 4 demonstrates that the disease-free Rosenzweig–MacArthur model shows spiral patterns. These spiral patterns can be analysed with respect to their characteristic spatial sizes and orientations of the populations. Despite the model having no particular rotational symmetries, we observe spiral patterns; however, these patterns are lost once the disease is introduced into the predator species. Earlier studies [38–40] showed that the preservation of spiral patterns can occur with small differences between either the growth rates or the diffusion coefficients; here, however, we noticed that the spiral patterns can be prevented completely by introducing a transmissible disease in one species.

Due to the complexity of the dynamics, very little work has been done on diffusive eco-epidemic models in three dimensions. The models discussed here can be used to study other eco-epidemic scenarios, with extensions to patchy landscape invasions or chaos in multi-species models [41]. Temporal models demonstrate interesting dynamics, but spatial models are more suited to ecological scenarios. Future work will extend our models to more nuanced situations in eco-epidemiology such as food webs and competitor-mediated coexistence.

Our model has some limitations, which should be acknowledged. Modelling a full eco-epidemiological system is challenging, due to the number of factors involved. We assumed mass-action transmission for the infection between predators. Only the susceptible predator was able to find additional sources of food, on the assumption that the infected predator was too sick to do so; this may not hold in all cases. We also assumed that spatial movement of all three populations was through diffusion, when the reality is much more complex.

Our work illustrates the utility of combining epidemiological models with ecological models in order to gain more insight into the spread of disease through time while populations simultaneously diffuse spatially. Periodic patterns may sustain the disease, although this at least may be predictable. Conversely, chaotic patterns may cause the disease to become eradicated, although it is important to note that this scenario loses predictability.

CRediT authorship contribution statement

Nayana Mukherjee: Software, Writing – original draft. **Stacey R. Smith?:** Writing – review & editing. **Mainul Haque:** Conceptualization, Methodology, Supervision.

Declaration of competing interest

The authors declare that they have no known competing financial interests or personal relationships that could have appeared to influence the work reported in this paper.

Data availability

No data was used for the research described in the article.

Acknowledgment

SRS? is supported by an NSERC Discovery Grant. For citation purposes, please note that the question mark in “Smith?” is part of her name.

References

[1] Buck JC, Ripple WJ. Infectious agents trigger trophic cascades. Trends Ecol Evol 2017;32(9):681–94.
[2] Friman VP, Lindstedt C, Hiltunen T, Laakso J, Mappes J. Predation on multiple trophic levels shapes the evolution of pathogen virulence. PLoS One 2009;4(8):e6761.
[3] Ross PS. The role of immunotoxic environmental contaminants in facilitating the emergence of infectious diseases in marine mammals. Hum Ecol Risk Assess Int J 2002;8(2):277–92.
[4] Sanderson CE, Alexander KA. Unchartered waters: Climate change likely to intensify infectious disease outbreaks causing mass mortality events in marine mammals. Glob Chang Biol 2020;26(8):4284–301.

[5] Selakovic S, de Ruiter PC, Heesterbeek H. Infectious disease agents mediate interaction in food webs and ecosystems. Proc R Soc B Biol Sci 2014;281(1777):20132709.
[6] Altizer S, Ostfeld RS, Johnson PT, Kutz S, Harvell CD. Climate change and infectious diseases: from evidence to a predictive framework. Science 2013;341(6145):514–9.
[7] Combe M, Velvin CJ, Morris A, Garchitorena A, Carolan K, Sanhueza D, et al. Global and local environmental changes as drivers of Buruli ulcer emergence: Environmental changes and infectious disease. Emerg Microbes Infect 2017;6(1):1.
[8] Yeni DK, Büyük F, Ashraf A, Shah MS. Tularemia: a re-emerging tick-borne infectious disease. Folia Microbiol 2021;66(1):1–4.
[9] Crowl TA, Crist TO, Parmenter RR, Belovsky G, Lugo AE. The spread of invasive species and infectious disease as drivers of ecosystem change. Front Ecol Environ 2008;6(5):238–46.
[10] Hethcote Herbert W. The mathematics of infectious diseases. SIAM Rev 2000;42(4):599–653. http://dx.doi.org/10.1137/S0036144500371907.
[11] Diekmann O, Heesterbeek JAP, Metz JAJ. On the definition and the computation of the basic reproduction ratio R0 in models for infectious diseases in heterogeneous populations. J Math Biol 1990;28:365–82.
[12] Kermack William Ogilvy, McKendrick AG, Walker Gilbert Thomas. A contribution to the mathematical theory of epidemics. Proc R Soc Lond Ser A Contain Pap Math Phys Charact 1927;115(772):700–21. http://dx.doi.org/10.1098/rspa.1927.0118.
[13] Morozov A. Modelling in ecology, epidemiology and ecoepidemiology: Introduction to the special issue. Math Model Nat Phenom 2015;10(2):1–4. http://dx.doi.org/10.1051/mmnp/201510201.
[14] Morozov A. Revealing the role of predator-dependent disease transmission in the epidemiology of a wildlife infection: a model study. Theor Ecol 2011;5:517–32.
[15] Holt RD, Roy M. Predation can increase the prevalence of infectious disease. Am Nat 2007;169:690–9.
[16] Seo G, Wolkowicz GS. Sensitivity of the dynamics of the general Rosenzweig–MacArthur model to the mathematical form of the functional response: a bifurcation theory approach. J Math Biol 2018;76(7):1873–906.
[17] Tang L, Zhou Y, Wang L, Purkayastha S, Zhang L, He J, et al. A review of multi-compartment infectious disease models. Int Stat Rev 2020;88(2):462–513.
[18] Xiao Y, Chen L. Modeling and analysis of a Predator–Prey model with disease in the prey. Math Biosci 2001;171(1):59–82. http://dx.doi.org/10.1016/S0025-5564(01)00049-9.
[19] Mukherjee D. Uniform persistence in a generalized Predator–Prey system with parasitic infection. Biosystems 1998;47(3):149–55. http://dx.doi.org/10.1016/S0303-2647(98)00022-7.
[20] Gulland FMD. The impact of infectious diseases on wild animal populations — a review. In: Grenfell BT, Dobson AP, editors. Ecology and infectious diseases in natural populations. Cambridge Univ. Press; 1995.
[21] Festenberg NV, Gross T, Blasius B. Seasonal forcing drives spatio-temporal pattern formation in rabies epidemics. Math Modell Nat Phenomena 2007;2(4):63–73.
[22] Murray JD. Mathematical biology. Heidelberg: Springer; 1989.
[23] Turing AM. The chemical basis of morphogenesis. Philos Trans R Soc Lond B 1952;237:37–72.
[24] Petrovskii SV, Malchow H. A minimal model of pattern formation in a Predator–Prey system. Math Comput Modelling 1999;29(8):49–63. http://dx.doi.org/10.1016/S0895-7177(99)00070-9.
[25] Banerjee M, Petrovskii S. Self-organised spatial patterns and chaos in a ratio-dependent Predator–Prey system. Theor Ecol 2011;4:37–53.
[26] Mukherjee N, Ghorai S, Banerjee M. Detection of turing patterns in a three species food chain model via amplitude equation. Commun Nonlinear Sci Numer Simul 2019;69:219–36.
[27] Chang Z, Xing X, Liu S, Meng X. Spatiotemporal dynamics for an impulsive eco-epidemiological system driven by canine distemper virus. Appl Math Comput 2021;402:126135.
[28] Lu Y, Xiao M, Chen G, Tao B, Chen S, Liu J. Turing instability analysis of marine planktonic ecosystem under the influence of spatial heterogeneity. In: 2021 33rd Chinese control and decision conference. IEEE; 2021, p. 5333–8.
[29] Anderson RM, May RM. The invasion, persistence and spread of infectious diseases within animal and plant communities. Philos Trans R Soc Lond B Biol Sci 1986;314(1167):533–70.
[30] Murray JD. Mathematical biology. New York: Springer; 1989.
[31] Tanner JT. The stability and intrinsic growth rates of prey and predator populations. Ecology 1975;56:855–67.
[32] Haque M. Existence of complex patterns in the Beddington–DeAngelis predator–prey model. Math Biosci 2012;239(2):179–90.
[33] Haque Mainul. A Predator–Prey model with disease in the predator species only. Nonlinear Anal RWA 2010;11:2224–36.
[34] Haque M, Greenhalgh D. When predator avoids infected prey: A model based theoretical studies. Math Med Biol A J IMA 2010;27:75–94.
[35] Alikakos ND. An application of the invariance principle to reaction–diffusion equations. J Differential Equations 1979;33:201–25.
[36] Cantrell RS, Cosner C, Hutson V. Permanence in ecological systems with spatial heterogeneity. Proc R Soc Edinb Sect A 1993;123:533–59.
[37] Mukherjee N, Ghorai S, Banerjee M. Cross-diffusion induced turing and non-turing patterns in Rosenzweig–MacArthur model. Lett Biomath 2019;6(1):1–22.
[38] Lin J, Sun H, Dong J. Emergence of sector and spiral patterns from a two-species mutualistic cross-feeding model. PLoS One 2022;17(10):e0276268.
[39] Volpert V, Petrovskii S. Reaction–diffusion waves in biology. Phys Life Rev 1571-0645 2009;6(4):267.
[40] Malchow H, Petrovskii SV, Venturino E. Spatiotemporal patterns in ecology and epidemiology. Theory, models, and simulations. Boca Raton, FL: Chapman & Hall/CRC Mathematical and Computational Biology Series, Chapman & Hall/CRC; 2008.
[41] Malchow H. Spatiotemporal patterns in ecology and epidemiology: theory, models, and simulation. Chapman and Hall/CRC; 2007.